Inferring the permeability field under embankments using hydraulic head measurements

Yaro S. Linnemann

March 2024

Head of Committee: prof. dr. Vanessa Magnanimo
Daily supervisor: dr. Hongyang Cheng
External supervisors: dr. Vera van Beek, dr. Bryant Robbins

Abstract

Dike failure poses a great risk to areas around rivers and coasts, one of the ways this can happen is piping. A difficulty in the prediction of piping is characterising the subsoil under the embankment, this study seeks to conceptualise a new way of doing this using groundwater head measurements. This is done with a combination of the GrainLearning inference tool and a groundwater flow model through the minimisation of the difference between predicted and synthetic measured hydraulic head profiles. This is done in two different ways: first through predicting the correlation length and standard deviation of the permeability random field and alternatively through fitting a specific field realisation including the random seed. The first method was not able to infer the field parameters. The second method achieved mixed results, with a relatively large error compared to the mean, but with some clear avenues for improvement. Practical applications could be found in selecting input fields that are consistent with field measurements when performing a Monte Carlo analysis on the embankment's piping safety.

Contents

1 Introduction

1.1 Background: Flood safety and piping

Flood safety is of critical concern the Netherlands and many other countries. Globally more than 500 million people live in river deltas [1]. This risk is mitigated by building dikes along rivers in order to allow for higher water levels without inundation. However these dikes are not infallible and can fail in different ways, among which are:[2] overflow, overtopping, micro- and macro-instability, erosion and backward erosion piping. The latter of which is the focus of this project.
Piping can be an insidious failure mechanism as it progresses in a manner that is difficult to detect until it is too late and the embankment suddenly collapses. The piping process happens as a result of groundwater flow under an embankment eroding a channel, see figure 1. According to Sellmeijer 1988[3] the process starts with seepage under an impervious structure, the embankment. Which then results in the movement of particles on the downstream side. This can then progressively erode a pipe under the embankment which may or may not reach an equilibrium. If this causes sufficient erosion under the embankment it can result in its collapse. Van Beek et al. 2012[4] describes the process as follows:

a The first step is when a sufficiently large hydraulic gradient under the embankment results in high water pressures, these then push against the impermeable top soil layer causing heave. Heave is the upwards expansion of the soil due to these pressures.

b The second step consists of water seepage through the cracks left in the impermeable top layer by the heave effect. This seepage can result in soil particles being moved upwards as well.

c The third step is the formation of a pipe through the top layer as a result of this seepage eroding the soil, the subsoil is then exposed to this pipe.

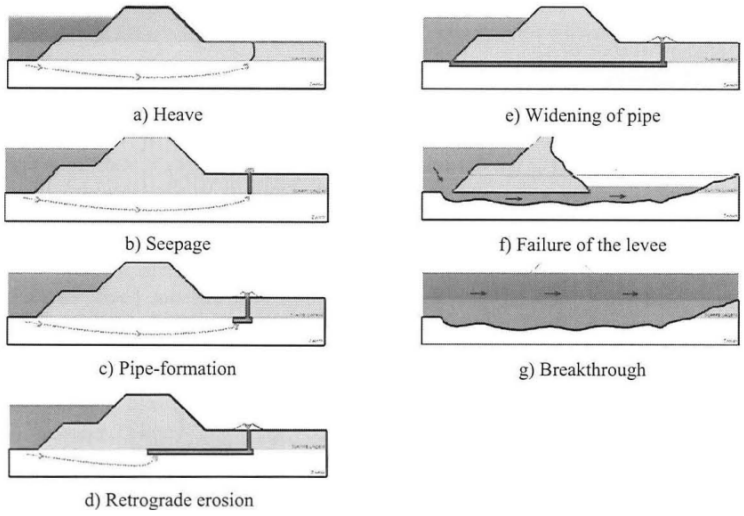

Figure 1: Image from [4] on the steps in piping

d This pipe can then erode further as the flow now takes sand particles with it, this will continue until it reaches an equilibrium.

e If the pipe erosion does not reach an equilibrium it will eventually reach the river allowing greater flow through it as the water is no longer limited by having to seep through soil.

f After the pipe becomes sufficiently wide the structure of the embankment will be compromised causing it to fail.

In order to limit the risks caused by this failure mechanism the empirical rules of Bligh, Lane and Sellmeijer are used to assess the safety of embankments in the Netherlands, although Bligh's rule is now considered to be insufficient in accurately determining safety according to research by Vrijling et al. [5].

New calculation rules for piping in Dutch engineering practice consider 60% of the 940km dikes studied to be insufficiently safe against piping [6]. If this sample is representative of the situation throughout the country it would take an immense amount of time and money to remedy.

However, there is a large amount of uncertainty regarding the material characteristics of the subsoil. These characteristics are spatially variable which further increases uncertainty about the embankment's safety level as complete information about the makeup and distribution of the soil is not available [7]. Decreasing the uncertainty about the makeup and distribution of the subsoil could tighten the range of possible safety factors and as a result allow for more accurate determination of whether a dike requires expensive renovations.

1.2 Current engineering practice

In order to characterise the soil there are two main methods in use: CPT and core samples. CPT is an in-situ soil investigation method where a cone is pushed into the soil at a steady rate while continuously measuring the resistance exerted by the soil on the CPT cone [8]. Empirical relations are then used to quickly generate a continuous soil profile of the measuring site. The weakness of this method is that the characterisation is indirect and can not determine all soil parameters [9], some of which are crucial to piping. A relatively recent development which utilises a similar concept to the CPT test called the hydraulic profiling tool (HPT), which can be used in the place of CPT to still get the permeability [10]. It does this by injecting water into the soil as it is inserted, the post processing can then provide a vertical profile of the soil permeability. Both the CPT and HPT have the limitation that their results are based on empirical relations rather than direct physical relations [10] [8].

The other main method is to simply take samples of the soil with a tool called the sampling tube[8] in order to directly and accurately determine all relevant soil characteristics at a laboratory. The downside is that it is a point measurement at a certain depth, which makes multiple samples necessary to find the soil layers. It is also a lot more time-consuming than the CPT/HPT. The problem with both of these methods is that they are point measurements in a heterogeneous medium. This makes it difficult to determine the safety level of a dike against piping with a high degree of certainty which can lead to over- or underestimation of required investments.

Both of these methods only provide point measurements, and in order to characterise the rest of the subsoil it is necessary to interpolate between these points. One such method in current engineering use is Kriging [9]. Kriging gives a best linear unbiased prediction at non-measurement points using a weighted average of nearby measurement points. A Kriged estimate $\hat{X}(\mathbf{x})$ of the value at point $\mathbf{x}$ on the random field X($\mathbf{x}$) with n observations is given by:

$$\hat{X}(\mathbf{x}) = \sum_{k=1}^{n} \beta_k X_k \tag{1}$$

Where β_k is the Kriging weight at point k. It can be determined using equation 2:

$$\mathbf{K}\beta = \mathbf{M} \tag{2}$$

Where $\mathbf{K}$ and $\mathbf{M}$ are as following:

$$\mathbf{K} = \begin{bmatrix} c_{11} & c_{12} & ... & c_{1n} & g_1(x_1) & g_2(x_1) & ... & g_m(x_1) \\ c_{21} & c_{22} & ... & c_{2n} & g_1(x_2) & g_2(x_2) & ... & g_m(x_2) \\ ... & ... & ... & ... & ... & ... & ... & ... \\ c_{n1} & c_{n2} & ... & c_{nn} & g_1(x_n) & g_2(x_n) & ... & g_m(x_n) \\ g_1(x_1) & g_1(x_2) & ... & g_1(x_n) & 0 & 0 & ... & 0 \\ g_2(x_1) & g_2(x_2) & ... & g_2(x_n) & 0 & 0 & ... & 0 \\ ... & ... & ... & ... & ... & ... & ... & ... \\ g_m(x_1) & g_m(x_2) & ... & g_m(x_n) & 0 & 0 & ... & 0 \end{bmatrix} \tag{3}$$

Where $c_i j$ is the covariance between X_i and X_j [9] and $g_i(x)$ is a function of $\mathbf{x}$, typically $g_1(x) = 1$, $g_2(x) = x$, $g_3(x) = x^2$ etc. β and $\mathbf{M}$ are defined as follows:

$$\beta = \begin{bmatrix} \beta_1 \\ \beta_2 \\ . \\ . \\ \beta_n \\ -\eta_1 \\ -\eta_2 \\ . \\ . \\ -\eta_m \end{bmatrix}, \mathbf{M} = \begin{bmatrix} C_1 x \\ C_2 x \\ . \\ . \\ C_n x \\ g_1 \\ g_2 \\ . \\ . \\ g_m \end{bmatrix} \tag{4}$$

Where η_i are the Lagrangian parameters used to solve the problem, they are not of physical importance.

1.3 Problem statement

The problem with the existing methods is that HPT tests are based on empirical relations rather than physical equations [10], and core samples can characterise the soil in a mostly undisturbed state but come at a large investment for each measurement. This means that it can be very expensive to properly determine an embankment's risk of piping when exposed to high water levels. Additionally both of these methods require an interpolation method such as Kriging, which introduces additional uncertainty.

In order to reduce the cost of ensuring an accurate view of the reliability of existing embankments this study will attempt to characterise the soil permeability field under a simulated embankment using ground water head "sensors".

1.4 Research gap

Previous studies have been conducted regarding the effect of uncertainty in the subsoil under embankments on the piping safety factor[11], through applying a random field to the soil properties. However, current methodology relies heavily on the use of CPT and core sampling, which tends to cost a lot. This often makes it impossible to reach the desired certainty about the subsoil within the project budget[12]. If the pre-existing core samples could be combined with a cheaper method for additional data gathering the affordable certainty would improve.

The goal of this thesis is to attempt to to characterise the soil property random field under an embankment from the groundwater flow through it. This groundwater flow would be determined using sensors that are much cheaper to place per unit than the cost of performing traditional types of subsurface characterisation such as CPT and core sampling. The intended result of combining traditional sampling with the sensors would be a better view of the subsoil for the same budget compared to exclusively using traditional sampling methods.

1.5 Research questions

The main objective is to develop a method that allows the determination of the characteristics of the soil property random field from groundwater flow measurements. The main research question used to guide this process is: "How can the soil permeability random field in under an embankment be characterised using groundwater flow measurements". In order to answer this research question the following subquestions have been posed:

1. What effect do the characteristics of the soil permeability random field have on the groundwater hydraulic head profile in the numerical piping model by Bryant Robbins? [13]
2. How can the characteristics length of the soil permeability random field be inferred from groundwater hydraulic head measurements?
3. How robust is this method at characterising the soil permeability random field?
4. How accurately can this method characterise the soil permeability random field?

1.6 Scope and approach

The scope of this project is limited to the subsoil under an embankment which is the domain of the failure mechanism piping. Additionally the project is based on pre-existing data and the model, and no field experiments have taken place. The project is a proof of concept focused on synthetic datasets in order to have full knowledge of the ground truth and be able to objectively evaluate the performance of the proposed methodology. The project goals will be approached by using inference software to minimise the difference between the synthetically observed hydraulic head profile and the hydraulic head profile output from many model runs, also referred to as samples in this report. Both the synthetic observations and the sample runs are performed using a groundwater flow model, using inputs given by the inference software.

1.7 Clear definition of the expected results

The desired result is a model or method that allows the determination of the soil property random field using the following information:

1. Dike geometry
2. Water levels
3. Groundwater head measurements at different points under the embankment
4. Upper and lower bounds of of field parameters (standard deviation and correlation length)

5. Estimate of mean permeability under the embankment

The desired output of this model or method is then an approximation of the subsoil permeability random field.

2 Methodology

2.1 General idea

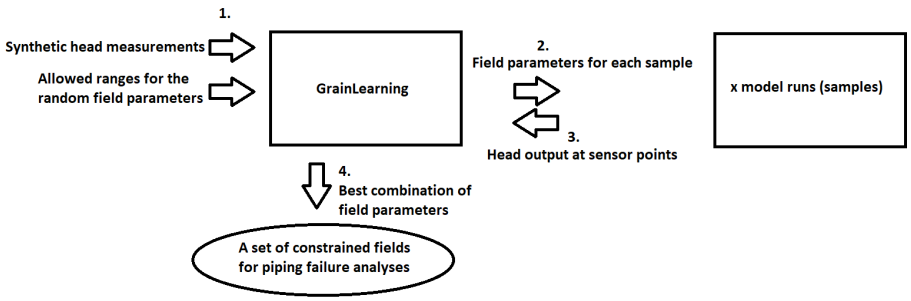

Figure 2: Flowchart of the general method of this project

This section describes the general flow of the combined inference system, the tools used for this will be described in sections 2.2 and 2.3, after which the two specific methods are described. See figure 2, the numbered steps in this flowchart will be explained in this section.

Each method starts with an input set of observed hydraulic head measurements, for the purpose of this study these are synthetically generated as per the project scope. This input is what the inference tool will attempt to approximate with model runs using varying input parameters. Besides this input observation there is also an input range of allowed parameters, with the parameters being dependent on the specific method, see sections 2.4 and 2.5. These inputs make up step 1.

With these parameter ranges a certain amount of runs of the mathematical model will be started using parameter values sampled from within the given ranges, this is step 2.

Step 3 consists of the sampled values being used in the physical model in order to generate sensor output for each parameter combination, this is then sent back to GrainLearning.

The characteristics of the permeability field are then determined by the model runs for which the difference in the hydraulic head profile from the ground truth is minimised, step 4 is GrainLearning performing this minimisation and outputting the corresponding parameter combination. When there is more than

one iteration steps 2&3 are repeated with resampled parameter combinations according to the results of the previous iteration.

2.2 The inference tool

This section will go further in depth about the inference tool used in this study, GrainLearning. There will first be a general explanation about what Bayesian inference is, and then a specific explanation about GrainLearning.

2.2.1 Bayesian Inference

Bayesian inference is a way in which the unknowns of a system can be inferred using observation of system outputs [14], based on Bayes' theorem. The equation used for Bayes' theorem can be seen below in equation 5.

$$p(A|B) = \frac{p(B|A)p(A)}{p(B)} \tag{5}$$

Where:

Table 1: Symbols for Bayes' theorem

$p(A \mid B)$	Probability of A given that B is true
$p(B \mid A)$	Probability of B given that A is true
$p(A)$	Probability of A
$p(B)$	Probability of B, used as normalising factor to make distribution sum to one

For the purpose of this study A is the model input which the system attempts to infer, while B is a specific hydraulic head profile which the model outputs. What this means is that the probability of a certain set of input parameters matches the unknown true input parameters given a certain output head profile can be determined using the product of the probability of that model input occurring and the probability of that specific head profile given this set of inputs. This can then be used to determine the most likely set of inputs for the observed output. Figure 3 [15] shows a visual representation of this process. Here in terms of this project the prior PDF represents the probability density function of the model input parameters, likelihood represents the likelihood of the model output given this model input. The posterior is then used as the result, as it gives a probability distribution of the likelihood of a specific combination of inputs given the model outputs. This is then used with the synthetic observations to find the most likely input combination that was used to get them.

2.2.2 GrainLearning

The tool used for the Bayesian inference in this project is the GrainLearning tool [16]. This tool was developed at the University of Twente by Cheng et al.

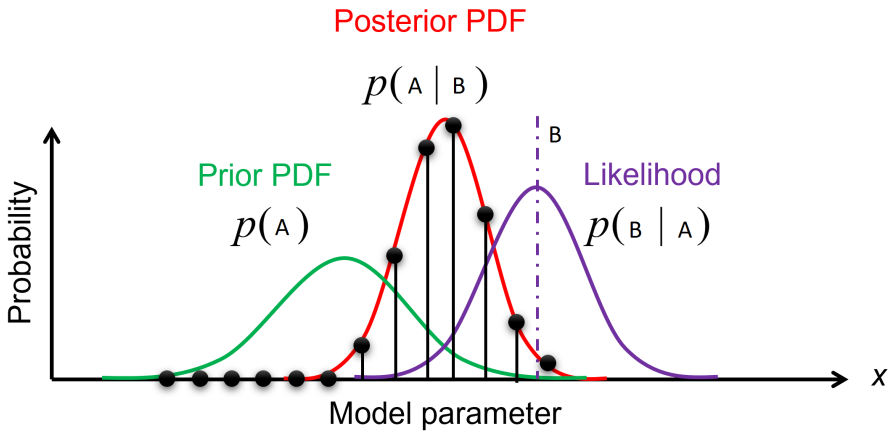

Figure 3: Graphical representation of the inference process, adapted from [15]

in order to infer parameters in geomechanical models. For the purpose of this study the Bayesian filtering module is used, which is based on Bayes' theorem as described above. The software follows the following steps in this project:

1. Generating initial samples within the allotted range using a Halton sequence
2. Running the mathematical model for each sample
3. Using model outputs to generate a new distribution $p(A \mid B)$
4. If there are more iterations to perform, generate new samples using distribution and repeat from step 2

When the tool is done, the distribution $p(A \mid B)$ is used to determine the most likely set of unknown input parameters for the input head profile.

2.3 The physical model

This section will explain the mathematical model used in this project, it starts with an explanation of the mathematics and then shortly goes into the specific software implementation used.

2.3.1 Random fields

In order to represent the uncertain and heterogeneous nature of the soil under an embankment a random field is used. A random field is a function that can take on any random value, governed by a probability density function[9], at each point of the field. The random field used in the model is a lognormal random

field, which means that the random field is governed by a lognormal probability density function. A lognormal field is governed by three key values [9]:

1. Field mean μ
2. Standard deviation σ
3. Correlation length (or CL) θ

Additionally the field is stationary, which means the key values as given above are independent of their location, and as such are the same for every point on the field. The mean and standard deviations are simply the characteristics of the probability density function that governs the field [9]. The correlation length is a length which determines how quickly correlation between two points on the field falls off with distance, a larger correlation length means points will be correlated at greater distances. When the model is used it will generate a realisation of the random field, a realisation is a field where each point has taken on a value from its probability density function. Where each point on a random field has a probability density function, each point on a random field realisation has a value.

2.3.2 Groundwater flow

Because this project considers ground water flow under an embankment in which the piping process has not been initialised yet the only relevant domain for water flow is the soil domain. An additional assumption is that the hydraulic conductivity is isotropic, which means that it is the same in both x and y directions. The flow is also steady, which means that there is no time dependence, and laminar which means all flow is in the primary direction without any turbulence. The groundwater flow is then governed by the Laplace equation, which is as follows [13]:

$$\frac{\partial}{\partial x}\Big(k\frac{\partial h}{\partial x}\Big) + \frac{\partial}{\partial y}\Big(k\frac{\partial h}{\partial y}\Big) = 0, \tag{6}$$

Where x and y are the axes of the plane, k is the hydraulic conductivity (permeability) and h is the total head. As described in the paper by Robbins and Griffiths [13], the FEM discretisation of equation 6 is then performed using the Galerkin weighted residual method, see equation 7.

$$[K_e]\{H\} = \{Q\}, \tag{7}$$

Where $\{H\}$ and $\{Q\}$ are the total head and water flow at each node, and $[K_e]$ for the situation with only a soil domain and isotropic permeability is as follows:

$$[K_e] = \sum_{\Omega} \int_{\Omega} k\Big(\frac{\partial N_i}{\partial x}\frac{\partial N_j}{\partial x} + \frac{\partial N_i}{\partial y}\frac{\partial N_j}{\partial y}\Big)d\Omega \tag{8}$$

Where Ω is the model domain and N_i and N_j are FEM element shape functions.

2.3.3 The RBEP2D model

The implementation of the mathematical model used in this project is the implementation by Bryant Robbins, as described in the papers [13] and [11]. This is originally a backwards erosion piping model which uses a random field for the subsoil permeability field under an embankment to analyse its vulnerability to backwards erosion piping. Several alterations have been made to this model in order to make it suitable for this project. The most important ones are:

Removal of the piping component
Characterising the embankment as done in this project is intended to be done at a point where there is no pipe forming yet, because the model was designed to simulate pipe progression this component had to be disabled. This changes the problem to only include a soil domain and reduces equation 14 from paper [13] to equation 8.

Simulation of sensor output
The model initially has the option to save the hydraulic head at every point, however for the purpose of this study only selected simulated sensor points are of interest, the output is changed to match this. This is the output from the mathematical model to GrainLearning.

2.4 Parameter inference method

The inference tool and mathematical model as described above can be used to characterise the subsoil permeability field in multiple different ways, the first method that was investigated in this research is the parameter inference method. Here the goal is to attempt to characterise the field by inferring the random field parameters that govern it, in this case the correlation length and standard deviation of the permeability. This section describes this process as it is applied in this project. The results of this method can be found in section 3.1.

2.4.1 Assumptions and constants

The following information counts for every case using the parameter inference method, unless stated otherwise:

1. The model domain for RBEP2D is 1D
2. The amount of sensor points is 20
3. Each model cell is 0.125m by 0.125m
4. The fit parameters are the correlation length θ and standard deviation σ of the subsoil permeability field, both in logscale
5. The ground truth logscale correlation length is 0.15 log(m), with a range between -0.5 and 0.5 log(m)

6. The ground truth logscale standard deviation is -4.6 log(m/s), with a range between -4 and -5.5 log(m/s)
7. The mean permeability in logscale is -5 log(m/s)
8. The seed is randomised by the RBEP2D program for each RBEP2D run
9. The amount of GrainLearning iterations is 5

A visual representation of the model domain can be seen in figure 4, here the red markings are the sensor points where the hydraulic head is output by the model. The domain is 80x1 grid spaces and the sensors are 4 grid points apart.

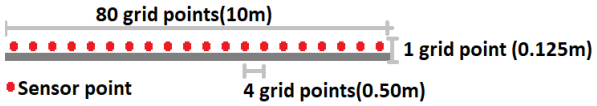

Figure 4: General model domain for the 1D Parameter Inference Method

2.4.2 Workflow of the parameter inference method

The following workflow was used in the parameter inference method:
First the RBEP2D model is ran once with the ground truth parameters in order to generate the linear observation file for GrainLearning.
Then 5 iterations of 300 samples are used to infer the standard deviation and correlation length.

2.4.3 Cases of the parameter inference method

In the exploration of this method a number of cases were investigated, with each one following a different approach in how to minimise the difference between the observations and model samples. Here $\hat{h}_r(s)$ is the raw head profile as output by RBEP2D, $\hat{h}_p(s)$ is the processed head profile which is read by GrainLearning and $\hat{h}_0(s)$ is the head profile in the homogeneous case with one uniform permeability, where s is the sensor point index.

Case 1
In case 1 the output time series from the sensors are directly used in grainlearning without any prior processing, see equation 9.For this first case the sensor count consists of 10 evenly spaced sensors rather than 20, see figure 5.

$$\begin{aligned} &\hat{h}_p(s) = \hat{h}_r(s) \\ &s \in N, s \leq 10 \end{aligned} \tag{9}$$

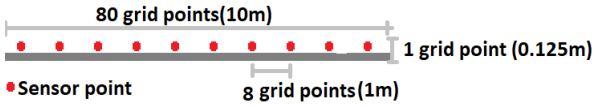

Figure 5: Model domain for case 1 of the 1D Parameter Inference Method

Case 2

In case 2 the output time series from the sensors are also directly used in Grain-Learning as in case 1, see equation 10. The difference from case 1 is that this case uses the standard sensor count of 20.

$$\begin{aligned} \hat{h}_p(s) &= \hat{h}_r(s) \\ s &\in N, s \leq 20 \end{aligned} \tag{10}$$

Case 3

In case 3 the output time series from the sensors are not directly used in Grain-Learning, they are first pre-processed such that each time series going into GrainLearning consists of the difference between two adjacent sensors (deltas), see equation 11. The reasoning being that this would give a more direct view of the soil permeability between the two.

$$\begin{aligned} \hat{h}_p(s) &= \hat{h}_r(s+1) - \hat{h}_r(s) \\ s &\in N, s \leq 20 \end{aligned} \tag{11}$$

Case 4

In case 4 the time series are pre-processed by taking the absolute difference between the sensor time series from the model as used in the inference and the time series from a separate run with a homogeneous permeability, see equation 12. The idea behind this case is to get the effect of the random field when compared to a homogeneous situation in order to get the parameters of said field.

$$\begin{aligned} \hat{h}_p(s) &= \hat{h}_r(s) - \hat{h}_0(s) \\ s &\in N, s \leq 20 \end{aligned} \tag{12}$$

Case 5

Case 5 combines case 3 and case 4 in order to get the difference between the deltas in the heterogeneous case and homogeneous case, see equation 13. The goal is to combine the effects of these two cases to completely isolate the random field's effects.

$$\begin{aligned} \hat{h}_p(s) &= (\hat{h}_r(s+1) - \hat{h}_r(s)) - (\hat{h}_0(s+1) - \hat{h}_0(s)) \\ s &\in N, s \leq 20 \end{aligned} \tag{13}$$

Case 6

Case 6 makes significant changes to the parameter inference method, instead of using the sensor measurements it uses the mean and standard deviation of

the sensor measurement deltas, see equation 14. This is done in order to reduce the effect of the randomised seed on the outcome by removing the influence of individual differences and only looking at the whole.

$$\begin{aligned} \hat{h}_p(1) &= mean(\hat{h}_r(s+1) - \hat{h}_r(s)) \\ \hat{h}_p(2) &= std(\hat{h}_r(s+1) - \hat{h}_r(s)) \\ s &\in N, s \leq 20 \end{aligned} \tag{14}$$

Case 7
Case 7 is similar to case 6 in that it uses statistical values derived from sensor results instead of using the sensor results themselves, only this time it takes the mean of both the direct heads and the head deltas, see equation 15.

$$\begin{aligned} \hat{h}_p(1) &= mean(\hat{h}_r(s+1) - \hat{h}_r(s)) \\ \hat{h}_p(2) &= mean(\hat{h}_r(s)) \\ s &\in N, s \leq 20 \end{aligned} \tag{15}$$

Table 2: List of cases for the parameter inference method as described in section 2.4.3

Case	Description
1	Reduced to 10 sensors, no pre-processing
2	No pre-processing
3	Head deltas
4	Head difference between random field and homogeneous
5	Delta difference between random field and homogeneous
6	Mean & std of deltas
7	Mean of head and deltas

2.4.4 Robustness and accuracy tests

The following tests were used to determine the effectiveness and robustness of the parameter inference method, for each of the tests the result will be an output standard deviation and correlation length from the inference which can be compared to the ground truth. For each test the cases are ran for 100 different realisations of the true field in order to get statistical measures of the method effectiveness

Default test
In the default test the different cases for the parameter inference method are used with the parameter ground truth and range values as given in section 2.4.1.

Large range test

In the large range test the same ground truth is used as in the default test, however, the ranges given to GrainLearning are expanded. The goal of this test is to find out whether the system can narrow the results down from a wider search.

Shift test
In the shift test the allowable parameter ranges are the same as in the default test, however, the ground truth is shifted when compared to the default values. This is done to determine whether the output results are properly approximating the ground truth, or whether they happen to be close by coincidence.

2.5 Field inference method

The field inference method is the second way in which the field is characterised in this study. The field inference method seeks to infer the field realisation directly, rather than characterising it by its correlation length and standard deviation. This is achieved by making the seed one of the fit parameters GrainLearning seeks to infer. Because every parameter combination results in a completely new field even for small differences, this does mean the iteration count has to be set to 1, as multiple iterations would not make any sense. The results for the 1D and 2D Field Inference Method can be found in sections 3.2 and 3.3.1.

2.5.1 Assumptions and constants

The following information counts for every case using the field inference method, unless stated otherwise:

1. The ground truth logscale correlation length is 0.15 log(m), with a range between -0.5 and 0.5 log(m)
2. The ground truth logscale standard deviation is -4.6 log(m/s), with a range between -4 and -5.5 log(m/s)
3. The mean permeability in logscale is -5 log(m/s)
4. The seed is a fit parameter for GrainLearning
5. The amount of GrainLearning iterations is 1
6. Each model cell is 0.125m by 0.125m

2.5.2 Workflow of the field inference method

The following workflow is used in the field inference method:
First the RBEP2D model is ran once with ground truth parameters including the seed, both the sensor output and field realisation are saved to file. 1 iteration of grainlearning is then used to find a combination of parameters, and therefore a field realisation that gives the best fit for the sensor output.

2.5.3 Cases of the field inference method

The field inference method contains two cases: a 1D case and a 2D case, because of the difference between the two, not all tests will be exactly equal, however whenever possible the tests are aligned.

1D case
The 1D case largely follows the parameter inference method in its setup, the model domain is 80 cells long and one cell wide. The amount of sensor points is 20 by default, but will be varied in some of the tests. The amount of samples is high to increase the chance of finding the right combination using the seed fit.

2D case
The 2D case uses a model domain of 80 by 80 cells, the sensors are arranged in a square shape with even spacing along each axis. The amount of samples will generally be less than in the 1D case, because of the much larger computational cost.

2.5.4 Robustness and accuracy tests (1D)

See table 3 for all the varied parameters and their values, the default values are given in **bold**. For each test one of the parameters will be varied while the other parameters are kept at their default values, in order to isolate the effect of each individual parameter.

Table 3: Parameter values used in testing of the 1D field inference method

Parameter					
Sensor count	5	10	**20**		
Sample count	625	1250	2500	**5000**	10000
Correlation length ground truth (log(m))	-0.15	0	**0.15**	0.3	0.45
Standard deviation ground truth (log(m/s))	-5.1	-4.85	**-4.6**	-4.35	-4.1

2.5.5 Robustness and accuracy tests (2D)

As with the 1D test, the parameters are varied one-by-one, they can be seen in table 4. The correlation length and standard deviation follow the same range as for 1D, but the sensor and sample counts are different to account for the different model domain and computational cost.

3 Results

3.1 1D parameter inference method

In this section the results of each test for the parameter inference method will be discussed, starting with an in-depth look per test and finishing with a summary.

Table 4: Parameter values used in testing of the 2D field inference method

Parameter					
Sensor count	4	9	**16**	25	36
Sample count	250	500	**1000**	2000	4000
Correlation length ground truth (log(m))	-0.15	0	**0.15**	0.3	0.45
Standard deviation ground truth (log(m/s))	-5.1	-4.85	**-4.6**	-4.35	-4.1

3.1.1 Default test

See table 5, this table shows the results for the default test with the input parameters as given in 2.4.1. Notable about these results is that the correlation lengths all tend to go towards the center of the range, which is at 0. The results for the standard deviation of the soil permeability random field also tend to be around the center of the range which is -4.75. For the correlation length case 3 appears to give a good result for the correlation length in this specific test. The random field standard deviation results appear to be decent for test 3, 6 and 7, although these results do have a large variance.

Table 5: Results of the default test for the parameter inference method

Test case	Mean CL (m)	STD CL(m)	Mean k (m/s)	STD k (m/s)
1	0.0434	0.128	-4.84	0.299
2	0.0526	0.129	-4.81	0.304
3	0.162	0.033	-4.51	0.176
4	-0.0055	0.159	-4.98	0.342
5	0.0673	0.0751	-5.25	0.187
6	0.0256	0.0552	-4.62	0.218
7	0.0424	0.105	-4.69	0.245

3.1.2 Shift test

See table 6, this test has the same range as the previous test, but now the ground truths are shifted to 0.3 and -5.1 for the correlation length and standard deviation respectively. As can be seen in the mean CL column, the correlation length still tends to be around the middle of the range rather than the ground truth, case 3 which previously seemed promising also appears to stick around 0.15 instead of following the ground truth. This means the good result in the default test was likely to be a coincidence. The field standard deviation results do all move along with the ground truth shift, suggesting that these do in fact infer a value rather than moving towards the center of the range.

Table 6: Results of the shift test for the parameter inference method

Test case	Mean CL (m)	STD CL(m)	Mean k	STD k
1	-0.0352	0.113	-5.08	0.24
2	-0.0224	0.113	-5.06	0.243
3	0.138	0.0525	-5.06	0.243
4	-0.0513	0.126	-5.16	0.241
5	0.0399	0.0882	-5.36	0.0748
6	0.0116	0.0565	-5.07	0.192
7	0.0495	0.104	-5.07	0.265

3.1.3 Large range test

See table 7, the large range test has the same ground truth as the default test, but the maximum correlation length and standard deviation given to Grain-Learning have been increased to $10^{1.5}$ and 10^{-3} respectively. This test shows that the correlation length moves along towards the new center of the range, although it does stay somewhere in between this and the ground truth. The standard deviation results generally stay much closer to the ground truth than the correlation length results do. The main exceptions here are cases 3, 6 and 7 which all move significantly towards the expanded part of the parameter range.

Table 7: Results of the large range test for the parameter inference method

Test case	Mean CL (log(m))	STD CL (log(m))	Mean k	STD k
1	0.591	0.209	-4.6	0.505
2	0.659	0.188	-4.54	0.561
3	0.746	0.114	-3.86	0.227
4	0.53	0.221	-4.87	0.496
5	0.849	0.177	-5.04	0.395
6	0.548	0.146	-4.23	0.285
7	0.553	0.241	-4.34	0.448

3.1.4 Summary of results

To summarise the results of the parameter inference method: None of the test cases performed well for each test regarding the correlation length, and it appears the results are centered around the center of the input range regardless of the ground truth.

For the standard deviation some of the test cases gave some decent results in the default and shift test, namely 3, 6 and 7. However when the range was increased the result of these also moved away from the ground truth.

3.2 1D field inference method

In this section the results of all the test cases for the 1D field inference method are showcased, the results are represented by the dimensionless value MAE/mean. MAE/mean is the mean absolute error divided by the mean permeability of the observed field, the mean absolute error is obtained by subtracting each point of the inferred field from that same point on the observation field and taking the absolute and mean of this difference.

$$MAE = \frac{1}{l} \sum_{n=1}^{l} |k_o(n) - k_i(n)| \tag{16}$$

Where:
k_o is the observed permeability at point n (m/s)
k_i is the inferred permeability at point n (m/s)
l is the amount of points

In the tables shown below for the results this quantity is then divided by the mean in order to get the MAE/mean, a dimensionless error measure normalised to the mean of the observed field. This error measure is determined over 100 separate inference runs, each with a different synthetic observation.

3.2.1 Visual inspection

In this visual inspection the inferred and true field of three different inferences of the default case will be shown and analysed: the result with the largest error, the result with the smallest error and the median result. Sensor points in the graph are marked with a black circle on the observation line. The normalised permeability on the y-axis of these graphs is the permeability divided by the mean of the observed field.

The smallest error
See figure 6, this figure shows the true and inferred field of the inference run where the MAE was the smallest. The MAE/mean in this figure is 0.70. Visually the fit between the simulations and synthetic observations looks like a somewhat close match, with the main deviation being the large peak in the synthetic observation around the middle of the field which is not present in the inferred field.

The median error
See figure 7, this figure shows the true and inferred field of the inference run with a median MAE. The MAE/mean in this figure is 1.15. Compared to the previous figure with the smallest MAE this figure shows a considerably worse fit to the observations, with very large differences in the downstream part of the field. A plausible explanation for the fact that this field was selected as best fit by GrainLearning is that the permeability peaks are of somewhat similar size

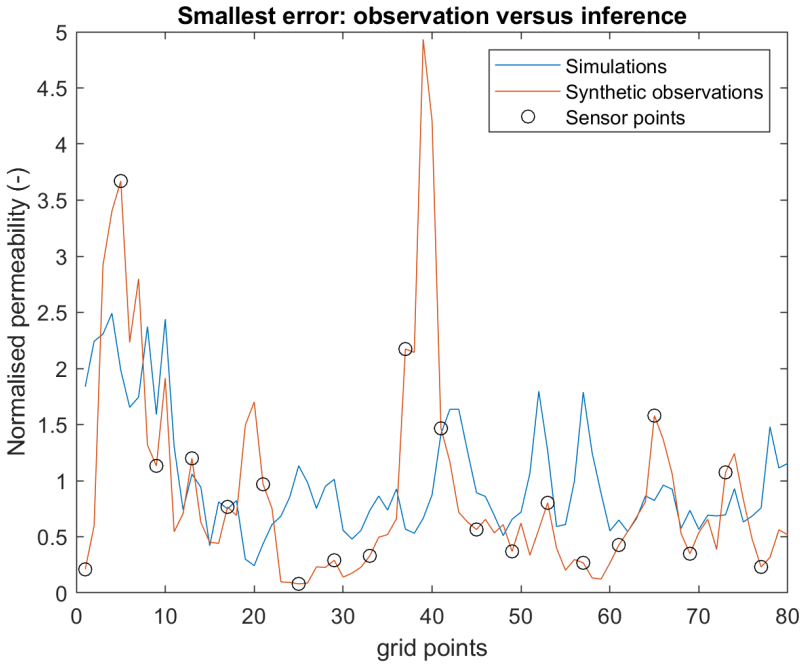

Figure 6: Inferred and observed permeability field for the 1D field inference method run with the smallest error

and in the same area between simulations and observations.

The largest error

See figure 8, this shows the field for which the mean absolute error was the largest. The MAE/mean for this inference run was 4.31. Notable is the extremely large spike in the synthetic observations, which is likely the cause for the weak fit. This shows a potential weakness to this method when applied to outlier fields with very large deviations compared to the standard deviation, where it is very unlikely for a random simulation field to have a similar spike in a similar location.

Summary of visual inspections

In summary: the visual inspections show how the fit can be a pretty close match to the observations, but it also shows how this is not the default situation, as even the figure for the median error showed two permeability field realisations with significant differences. The run with the largest error also suggests that there might be fields which are simply not realistic to infer with this method.

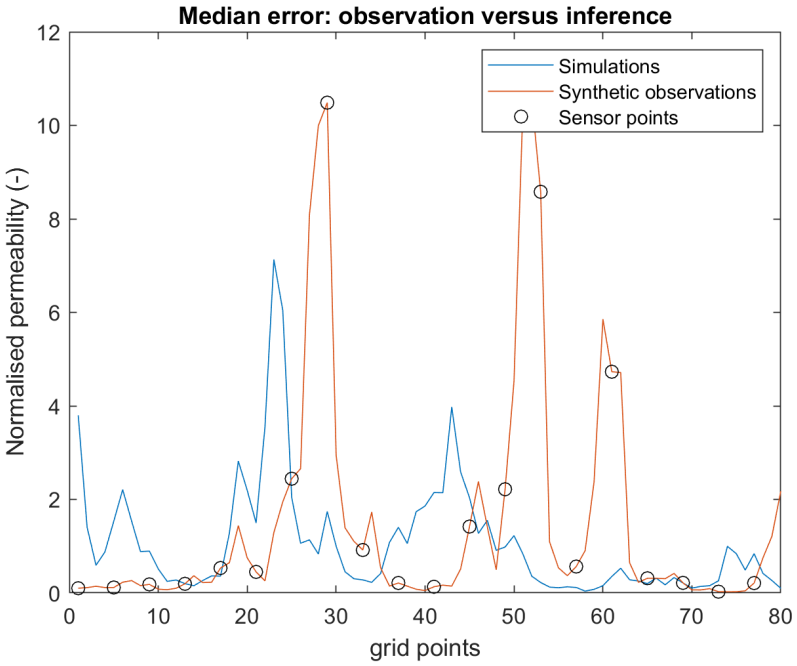

Figure 7: Inferred and observed permeability field for the 1D field inference method run with the median error

3.2.2 Run count test

See table 8, here it can be seen that unexpectedly the MAE/mean actually increases as the sample count increases. A plausible explanation for this is that a larger sample count leads to a better fit for the hydraulic head profile, which may not necessarily be a better fit for the MAE/mean. This is because the MAE/mean is more impacted by a large differences in peak permeabilities, whereas the head profile sees larger differences from the parts with a small permeability.

Table 8: Results of the sample count test for the 1D field inference method

Sample count	625	1250	2500	**5000**	10000
MAE/mean	1.2767	1.3299	1.4486	1.4161	1.4415

3.2.3 Correlation length test

See table 9, here it can be seen that as the correlation length increases, the mean error first decreases and then increases.

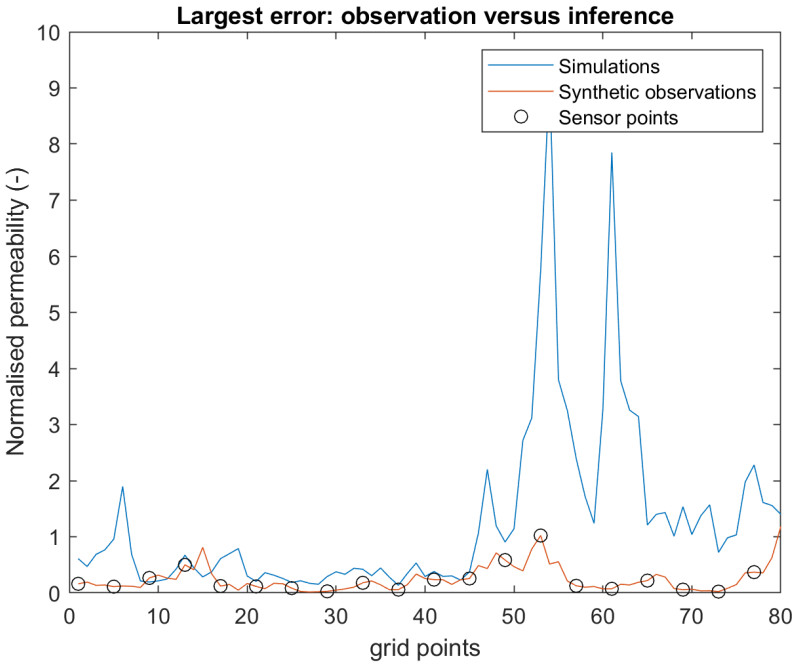

Figure 8: Inferred and observed permeability field for the 1D field inference method run with the largest error

This could imply that there is an optimal correlation length for the inference process around a correlation length of 1m. It is possible that this distance depends on the spacing of the sensor points, which would make the optimal sensor configuration dependent on the expected correlation length.

Another possibility is that it has nothing to do with the distance itself, but is simply a result of this correlation length being in the center of the range of values. This could increase the probability of a good fit as a larger amount of samples would be nearby compared to a ground truth on the edge of the sampling range.

Table 9: Results of the correlation length test for the 1D field inference method

Correlation length (log(m))	-0.15	0	**0.15**	0.3	0.45
MAE/mean	1.3803	1.2706	1.4161	1.5576	1.6587

3.2.4 Standard deviation test

See table 10, here it can be seen that as the standard deviation increases the error also increases drastically, however, the error when compared to the standard deviation stays at roughly the same value until it strongly increases for the largest standard deviation. What this means is that there is a positive correlation between the standard deviation and the error, and that for most of the range the error increases at the same rate as the standard deviation.

Table 10: Results of the standard deviation test for the 1D field inference method

standard deviation (log(m/s))	-5.1	-4.85	**-4.6**	-4.35	-4.1
MAE/mean	0.7242	1.0586	1.4161	1.8215	2.9405
MAE/std	1.1767	1.1184	1.1131	1.1201	1.7470

3.2.5 Sensor count test

See table 11, here it can be seen that there is no strong correlation between the mean absolute error and the sensor count that can be determined from these data points. Unexpectedly the correlation that is present would seem to point to a larger sensor count resulting in a larger error.

Table 11: Results of the sensor count test for the 1D field inference method

Sensor count	5	10	**20**	40
MAE/mean	1.3831	1.3723	1.4161	1.4138

3.2.6 Summary of results for 1D

To summarise: The mean absolute errors of the permeability field in the 1D field inference method are relatively large, with average values above the means of the observed fields. Results for the sensor count test show a small positive correlation between sensor count and error, and the sample count test shows a similar correlation between sample count and error. The correlation length shows what might be a "center of input range" effect, which could then logically also be present for the standard deviation. The error strongly increases with the standard deviation, at roughly the same rate as the standard deviation for most of the range.

3.3 2D field inference method

3.3.1 Visual inspection

As with the 1D situation, the inferred and true field will be compared here. These figures show the absolute error of the permeability field at each point, normalised to the mean permeability of the observed field. The colour scale is

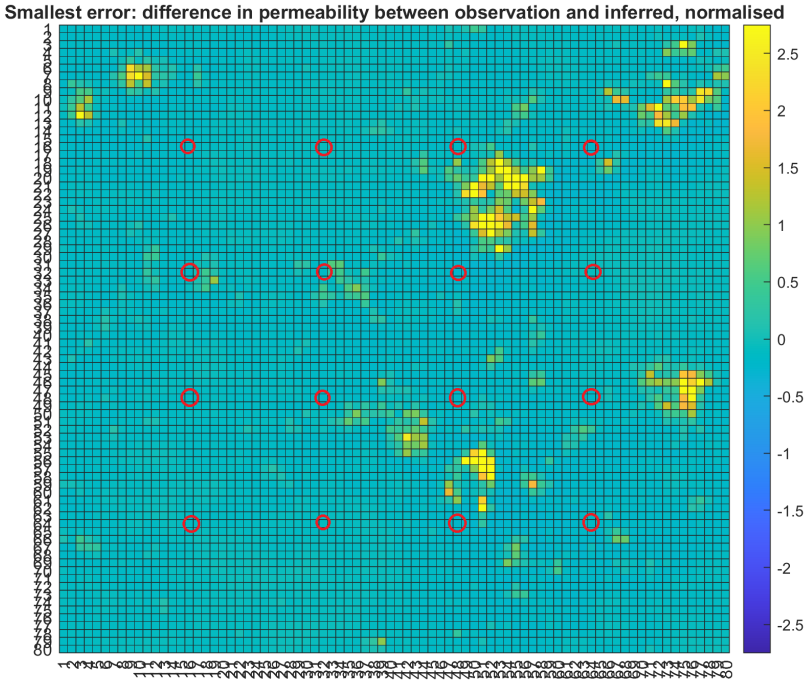

Figure 9: Difference between inferred and observed permeability field for the 2D field inference method run with the smallest error, normalised to true mean

limited to 2.75 times the mean for readability reasons and consistency between figures. Sensor locations are marked with a red circle around their grid point. Separate fields without subtraction can be found in the appendix.

The smallest error

See figure 9, this figure shows results which had the smallest mean absolute error. The MAE/mean for this inference run was 0.20. Visually it can be seen that this is a rather close fit, as the error/mean is near 0 for most of the field. There are a few groups with a relatively large error, all in the positive direction meaning that the observed permeability in these places was larger than the inferred permeability. There are not enough error areas to suggest a correlation with their locations and those of the sensors.

The median error

See figure 10, this figure shows the difference between the observed and inferred

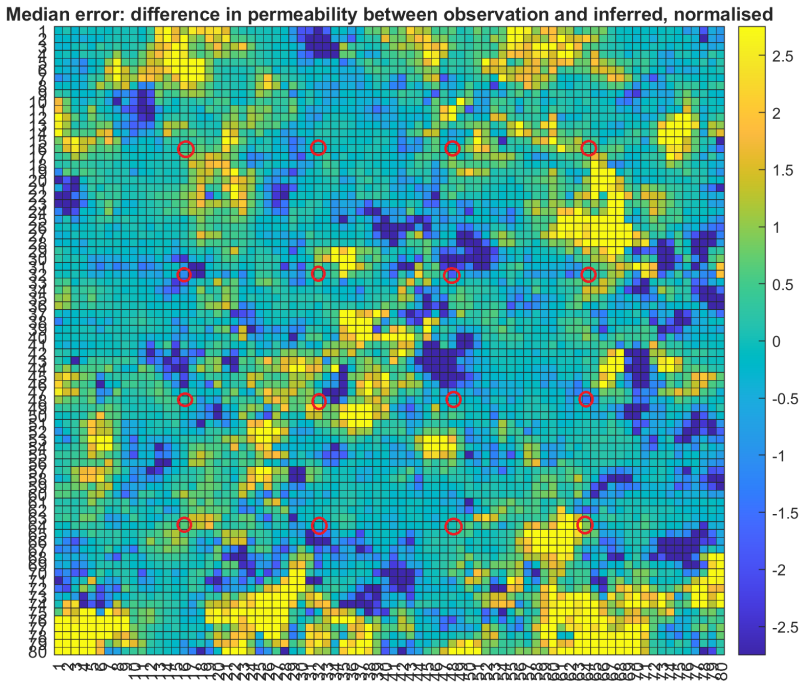

Figure 10: Difference between inferred and observed permeability field for the 2D field inference method run with the median error, normalised to true mean

permeability from the result with the median error. The MAE/mean in this figure was 1.11. Comparing this to the previous figure shows that there are much more error areas, which still mostly appear in the positive direction. Just as with the previous figure there is no visually discernible relationship between error and proximity to sensor points.

The largest error

See figure 11, this figure shows the difference between observed and inferred permeability for the result with the largest error. The MAE/mean for this figure was 1.91. The first noticeable thing is that the errors are concentrated in different areas from the previous figures, which might indicate that there is no clear standard location for larger errors. Compared to the previous figure the errors seem to be concentrated in larger groups, and both positive and negative errors are common.

Summary of visual inspections To summarise the visual inspections of

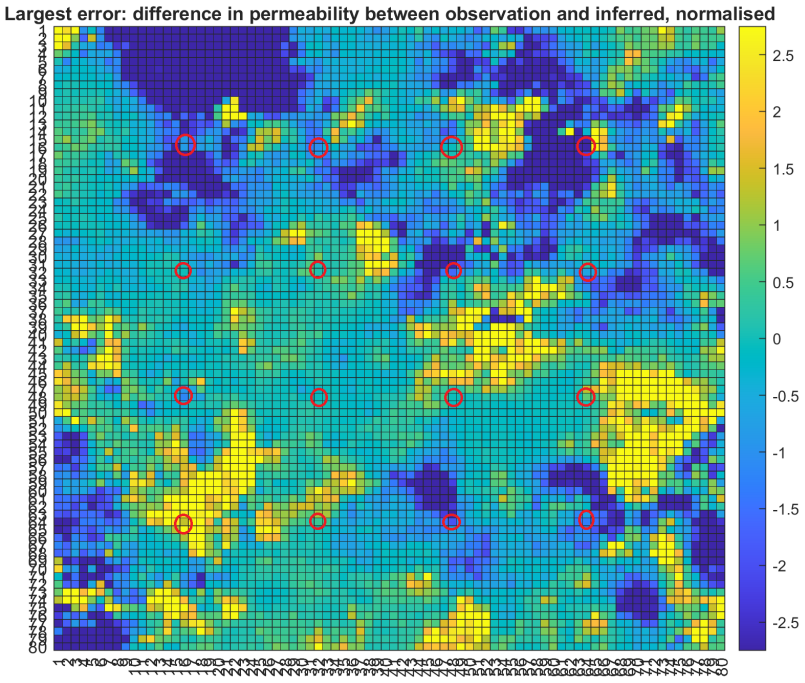

Figure 11: Difference between inferred and observed permeability field for the 2D field inference method run with the largest error, normalised to true mean

the results for the 2D field inference method, it seems that the distribution of large errors has no clearly defined pattern or area, and errors can happen anywhere. There is also a clear visual difference between the fields with smaller and larger errors.

3.3.2 Run count test

See table 12, here it can be seen that as with the 1D situation, the mean absolute error increases as the sample count increases. As with the 1D situation a plausible explanation for this is that for this range of sample counts the permeability fit is further optimised to get a closer fit for the head profile, but at the cost of a larger MAE/mean. Theoretically an infinite run count would get a perfect fit for the head profile, and as such the average permeability between sensor points would also match the observations. This means it is possible that the error initially increases with sample count and later decreases again after reaching a certain sample count.

Table 12: Results of the sample count test for the 2D field inference method

Sample count	250	500	**1000**	2000	4000
MAE/mean	1.0840	1.0966	1.1184	1.1190	1.1280

3.3.3 Correlation length test

See table 13, here it can be seen that as with the 1D situation there is a positive correlation between the correlation length and the error. The error minimum around a correlation length of 1m as seen in the 1D situation does not appear to be present in the 2D situation. This could mean there is no clear minimum in the correlation length for the 2D situation or it could be outside the range of experimental values.

Table 13: Results of the correlation length test for the 2D field inference method

Correlation length (log(m))	-0.3	-0.15	0	**0.15**	0.3	0.45
MAE/mean	1.0697	1.0725	1.0990	1.1184	1.1316	1.1514

3.3.4 Standard deviation test

See table 14, here it can be seen that as with the 1D situation and as expected, the error increases with the standard deviation of the permeability. Unlike the 1D situation, the error when normalised to the standard deviation shrinks as the standard deviation grows. This indicates that in the 2D situation the error increases at a lesser rate compared to the standard deviation, which could indicate the system deals relatively well with larger deviations.

Table 14: Results of the standard deviation test for the 2D field inference method

Standard deviation (log(m/s))	-5.1	-4.85	**-4.6**	-4.35	-4.1
MAE/mean	0.6570	0.9112	1.1184	1.3106	1.5050
MAE/std	0.9111	0.7532	0.5875	0.4746	0.4071

3.3.5 Sensor count test

See table 15, this shows a negative correlation between sensor count and mean absolute error. This relation is expected because a larger sensor count increases the amount of known information from the subsoil head profile, which then allows for a more accurate fit of the permeability field.

Table 15: Results of the sensor count test for the 2D field inference method

Sensor count	9	**16**	25	36	49
MAE/mean	1.1295	1.1184	1.1092	1.1073	1.0796

3.3.6 Summary of results for 2D and comparison to 1D

To summarise the results for the 2D field inference method: As with the 1D situation the errors are relatively large, the mean absolute errors are however lower than in the 1D situation. Due to the entirely different set up these values might not be directly comparable between the two. The sensor count test gave more expected results than in the 1D situation, showing a clear decrease of error with an increasing sensor count. The run count test shows the same increase as in the 1D situation, which could be attributed to the fact that a better fit for the hydraulic head profile based on the sensor data does not necessarily result in a better fit over the entire permeability field. The correlation length test does not show the same "center of range" effect as in the 1D situation, and is a simple increase of error with correlation length. The standard deviation test shows different results between the two experiments, whereas the error increases at roughly the same rate as the standard deviation in 1D, it increases at a slower rate in the 2D situation. This could indicate the 2D situation deals relatively well with larger standard deviations.

4 Discussion

4.1 Discussion of results

4.1.1 Parameter inference method

The parameter inference method was not able to make an acceptable prediction about the random field parameters in any of its cases. The suspected reason for this consists of two parts: The first component is that generating a new random field for every iteration makes it difficult to narrow down the proper combination

of parameters, as two field realisations with the exact same correlation length and standard deviation can be completely different, just as two field realisations with radically different correlation lengths and standard deviations could be exactly the same. The second component is that field parameters can never be exactly determined from a finite field realisation for the same reason as stated above.

One of the ways previous studies have done similar things to this one is the research into the Karhunen–Loève expansion (see [17][18][19][20]). The Karhunen–Loève expansion, or K-L expansion, is similar to this study's parameter inference method in that it uses model outputs to infer field parameters. In the case of the K-L expansion this is done with a series expansion which results in coefficients that replace the random field parameters.

4.1.2 Field inference method

The results as shown in the previous section show rather high mean absolute errors compared to the field mean, based on the results for the sample count and sensor count tests this could be improved by increasing these values. Theoretically as the sensor count and sample count go to infinity the mean absolute error should go to zero as the true field is one of those infinite samples.

Additionally the error measure is a rather harsh measure as it considers the error over the entire field while the inference only gets a set number of measurement points. Additionally the error measure directly looks at the permeability at each point instead of relative differences, which means that a field realisation with a relatively bad fit but a low mean will have a small error. A potentially more meaningful error measure is proposed in the section for future research.

Finally a difficulty of using the head profile to infer the permeability is that the head profile is determined by head drops between sensor points. What this means is that a given relative change on a section with a very low permeability will have a much greater effect on the head profile than the same relative change on a section with a very large permeability. This means the peaks of the permeability field are less likely to be accurately inferred. This could potentially cause issues when using the technique to characterise the subsoil in safety assessments.

4.2 Practical implications

From the final result a series of practical applications were devised and will be explained in this section.

4.2.1 Inferring the soil field

The most basic practical application of this technique is by applying it to what it was originally meant for in this project: Inferring the soil property field under an embankment. This would require creating a sensor setup and using it as input observation for the combined GrainLearning-RBEP2D model in order to

get a field inference. This field could then be used for safety assessment directly. The downside of this would be that for the sensor and sample count used in this study the error was still rather high which means that if it was to be used as measurement processing in a deterministic model these would have to be much higher in order to reduce this error.

4.2.2 Pre-filtering Monte Carlo

Another practical application which is related to the previous one is to use the system in order to pre-filter Monte Carlo runs for greater efficiency. This would entail feeding the information that is known about an embankment through sensor readings into this system, and using the output fields as input for a Monte Carlo run, thus narrowing down the uncertainty in the material properties which focuses the piping simulations on more likely scenarios. This has the potential of saving a lot of computing time as less time will be spent on expensive piping simulations, at the cost of simulation runs in this system which is much cheaper in comparison.

4.2.3 Verifying measurement system robustness

The final application of this system is to verify the robustness of existing measurement systems under embankments, an example of such a measurement system would be an early warning system. The way this would work is by putting head readings from the measurement setup into the combined GrainLearning-RBEP2D model. If the best fits according to this system show a large variety of possible fields it could indicate that the measurement setup is not robust, as the head outputs seem ambiguous to the inference system which means the same thing could happen in a real-life scenario. In that case the measurement system would need to be improved to ensure reliability.

5 Conclusion

A method was developed using the GrainLearning bayesian inference tool and the groundwater flow model which infers the soil permeability field from hydraulic head observations. The developed method shows relatively large absolute errors which could make it unsuitable as a method to get a field which is then treated as truth. It does however show potential for increasing this accuracy through increased sensor/sample count and could prove useful in other practical applications such as pre-filtering for Monte Carlo runs and verifying the robustness of sensor systems. The answer to the research question is "The soil permeability random field can be characterised through a Monte Carlo run where the best fit for the hydraulic head profile is selected".

5.1 Recommendations for future research

After concluding this research there were two obvious directions for future research outside of research into the potential practical applications listed above. The first of which would be to further judge the accuracy of the inference method itself, ideally by feeding the output field back into a piping model in order to get a safety factor. This could then be compared to the safety factor of the true field, which would provide a more practical error measure than was used in this research. The second recommendation is to research the combination of this sensor-based approach with traditional sampling methods, by assuming the permeability at sensor points to be known and using these as constraints for the random field. This would then ensure the sampled fields are at least somewhat consistent with what is known about the observed field.

References

[1] Robert Nicholls et al. "Delta Challenges and Trade-Offs from the Holocene to the Anthropocene". In: Jan. 2020, pp. 1–22. ISBN: 978-3-030-23516-1. DOI: 10.1007/978-3-030-23517-8_1.

[2] Expertisenetwerk Waterveiligheid. *Grondslagen voor hoogwater-bescherming*. ENW, 2017.

[3] J B Sellmeyer. *ON THE MECHANISM OF PIPING UNDER IMPERVIOUS STRUCTURES*. 1988.

[4] Van Beek et al. *Levee Failure Due to Piping: A Full-Scale Experiment*. 2012. URL: https://hdl.handle.net/20.500.11970/100310.

[5] P. Vrijling et al. *Piping - Realiteit of Rekenfout?* 2010. URL: www.enwinfo.nl.

[6] *PIPING, EEN BELANGRIJK FAALMECHANISME BIJ DIJKEN*. URL: https://pipingcontrol.nl/nl/content/piping-een-belangrijk-faalmechanisme-bij-dijken.

[7] M.A. Hicks and Jonathan Nuttall. "Influence of soil heterogeneity on geotechnical performance and uncertainty: a stochastic view on EC7". In: *Proc. 10th International Probabilistic Workshop, Stuttgart* (Jan. 2012), pp. 215–227.

[8] Muni Budhu. *Soil Mechanics Fundamentals*. John Wiley and Sons, 2015.

[9] Gordon A. Fenton and D. V. Griffiths. *Risk Assessment in Geotechnical Engineering*. John Wiley and Sons, 2008.

[10] Wesley McCall and Thomas M. Christy. "The Hydraulic Profiling Tool for Hydrogeologic Investigation of Unconsolidated Formations". In: *Groundwater Monitoring & Remediation* 40.3 (2020), pp. 89–103. DOI: https://doi.org/10.1111/gwmr.12399. eprint: https://ngwa.onlinelibrary.wiley.com/doi/pdf/10.1111/gwmr.12399. URL: https://ngwa.onlinelibrary.wiley.com/doi/abs/10.1111/gwmr.12399.

[11] B. A. Robbins, D. V. Griffiths, and Gordon A. Fenton. "Random finite element analysis of backward erosion piping". In: *Computers and Geotechnics* 138 (Oct. 2021). ISSN: 18737633. DOI: 10.1016/j.compgeo.2021.104322.

[12] Sarah Firouzianbandpey et al. "Effect of Spatial Correlation Length on the Interpretation of Normalized CPT Data Using a Kriging Approach". In: *Journal of Geotechnical and Geoenvironmental Engineering* 141 (June 2015), p. 04015052. DOI: 10.1061/(ASCE)GT.1943-5606.0001358.

[13] B. A. Robbins and D. V. Griffiths. "A two-dimensional, adaptive finite element approach for simulation of backward erosion piping". In: *Computers and Geotechnics* 129 (Jan. 2021). ISSN: 18737633. DOI: 10.1016/j.compgeo.2020.103820.

[14] *Bayesian filtering - GrainLearning documentation*. URL: https://grainlearning.readthedocs.io/en/latest/bayesian_filtering.html.

[15] *Bayesian filtering - GrainLearning documentation*. URL: https://grainlearning.readthedocs.io/en/latest/bayesian_filtering.html.

[16] *Welcome to GrainLearning's documentation! - GrainLearning documentation*. URL: https://grainlearning.readthedocs.io/en/latest/.

[17] Aronne Dell'Oca and Giovanni M. Porta. "Characterization of flow through random media via Karhunen–Loève expansion: an information theory perspective". In: *International Journal on Geomathematics* 11 (June 2020). DOI: https://doi.org/10.1007/s13137-020-00155-x.

[18] Felipe Uribe et al. "Bayesian inference with subset simulation in varying dimensions applied to the Karhunen–Loève expansion". In: *International Journal for Numerical Methods in Engineering* 122.18 (2021), pp. 5100–5127. DOI: https://doi.org/10.1002/nme.6758. eprint: https://onlinelibrary.wiley.com/doi/pdf/10.1002/nme.6758. URL: https://onlinelibrary.wiley.com/doi/abs/10.1002/nme.6758.

[19] Jonas Latz, Marvin Eisenberger, and Elisabeth Ullmann. "Fast sampling of parameterised Gaussian random fields". In: *Computer Methods in Applied Mechanics and Engineering* 348 (2019), pp. 978–1012. ISSN: 0045-7825. DOI: https://doi.org/10.1016/j.cma.2019.02.003. URL: https://www.sciencedirect.com/science/article/pii/S004578251930074X.

[20] Felipe Uribe et al. "Bayesian inference of random fields represented with the Karhunen–Loève expansion". In: *Computer Methods in Applied Mechanics and Engineering* 358 (2020), p. 112632. ISSN: 0045-7825. DOI: https://doi.org/10.1016/j.cma.2019.112632. URL: https://www.sciencedirect.com/science/article/pii/S004578251930516X.

Appendix: Separate fields from 2D test

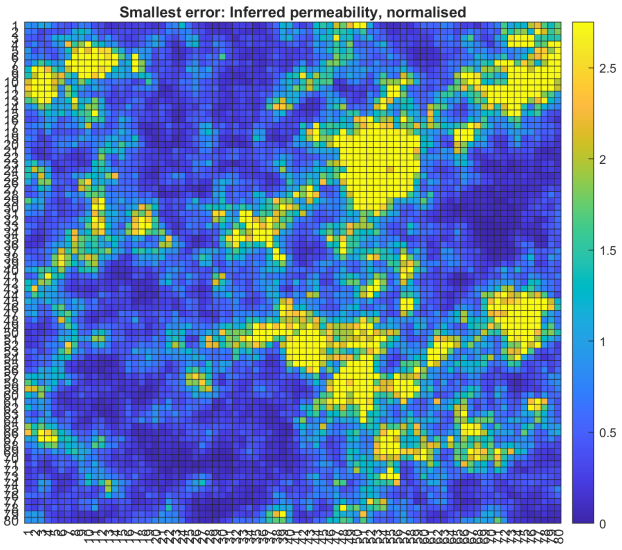

Figure 12: Inferred field with smallest error from 2D default test

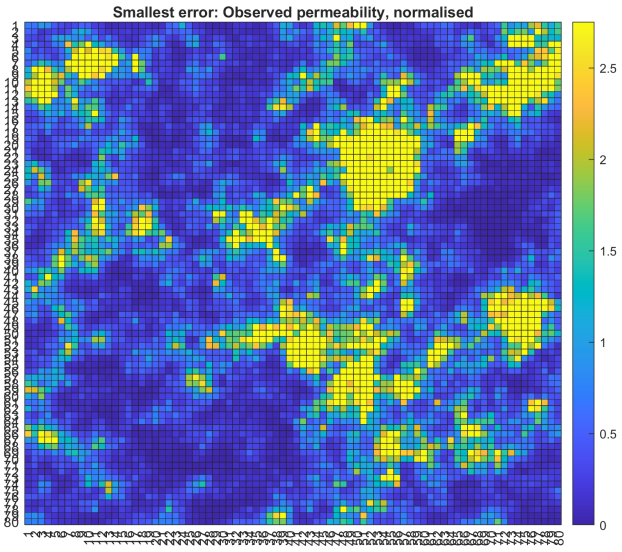

Figure 13: Observed field belonging to smallest error 2D default test

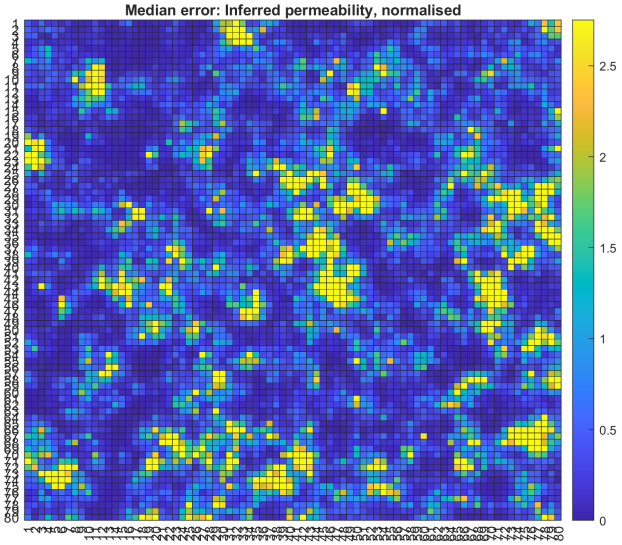

Figure 14: Inferred field with median error from 2D default test

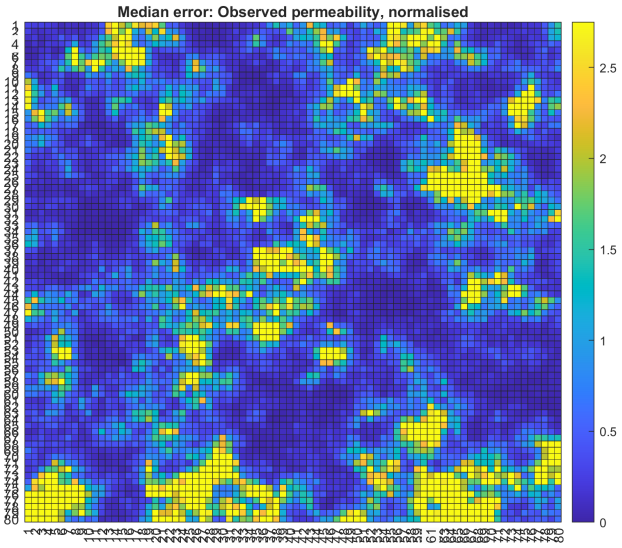

Figure 15: Inferred field with median error from 2D default test

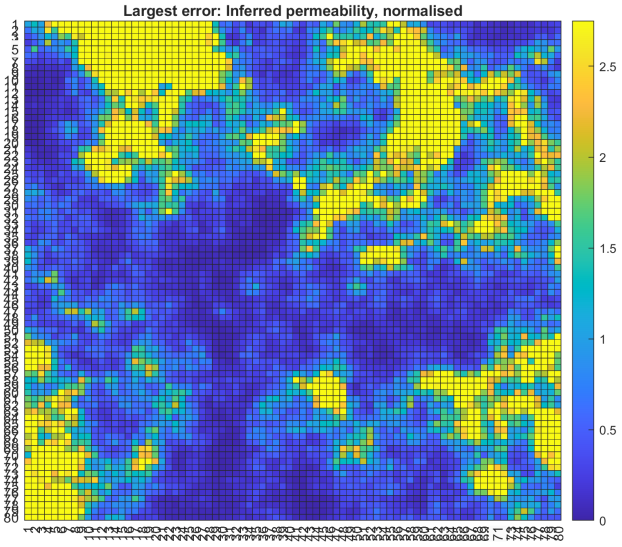

Figure 16: Inferred field with largest error from 2D default test

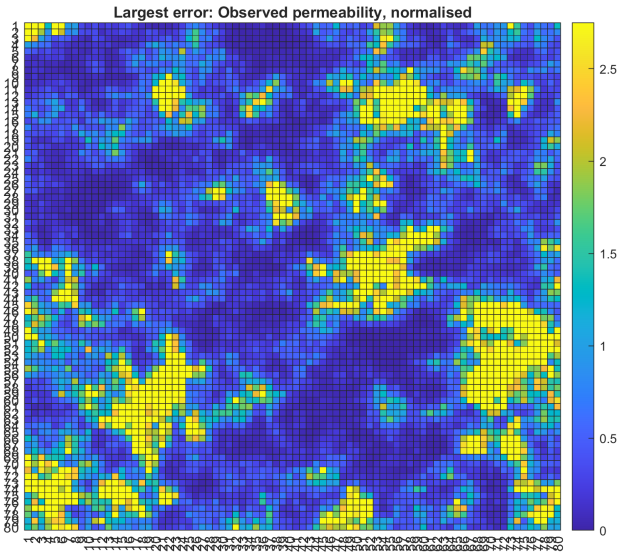

Figure 17: Inferred field with largest error from 2D default test